Climate Dynamics (2002) 19: 585–598
DOI 10.1007/s00382-002-0246-8

I.V. Kamenkovich · A.P. Sokolov · P.H. Stone

# An efficient climate model with a 3D ocean and statistical–dynamical atmosphere*

Received: 20 April 2001 / Accepted: 30 January 2002 / Published online: 29 May 2002


**Abstract** We describe a coupled climate model of intermediate complexity designed for use in global warming experiments. The atmospheric component is a two-dimensional (zonally averaged) statistical–dynamical model based on the Goddard Institute for Space Study's atmospheric general circulation model (GCM). In contrast with energy-balance models used in some climate models of intermediate complexity, this model includes full representation of the hydrological and momentum cycles. It also has parameterizations of the main physical processes, including a sophisticated radiation code. The ocean component is a coarse resolution ocean GCM with simplified global geometry based on the Geophysical Fluid Dynamics Laboratory modular ocean model. Because of the simplified geometry the resolution in the western boundary layers can be readily increased compared to conventional coarse resolution models, without increasing the model's computational requirements in a significant way. The ocean model's efficiency is also greatly increased by using a moderate degree of asynchronous coupling between the oceanic momentum and tracer fields. We demonstrate that this still allows an accurate simulation of transient behavior, including the seasonal cycle. A 100 years simulation with the model requires less than 8 hours on a state-of the art workstation. The main novelty of the model is therefore a combination of computational efficiency, statistical–dynamical atmosphere and 3D ocean. Long-term present-day climate simulations are carried out using the coupled model with and without flux adjustments, and with either the Gent-McWilliams (GM) parametrization scheme or horizontal diffusion (HD) in the ocean. Deep ocean temperatures systematically decrease in the runs without flux adjustment. We demonstrate that the mismatch between heat transports in the uncoupled states of two models is the main cause for the systematic drift. In addition, changes in the circulation and sea-ice formation also contribute to the drift. Flux adjustments in the freshwater fluxes are shown to have a stabilizing effect on the thermohaline circulation in the model, whereas the adjustments in the heat fluxes tend to weaken the global "conveyor". To evaluate the model's response to transient external forcing global warming simulations are also carried out with the flux-adjusted version of the coupled model. The coupled model reproduces reasonably well the behavior of more sophisticated coupled GCMs for both current climate and for the global warming scenarios.

## 1 Introduction

A systematic study of possible climate changes calls for carrying out a significant number of long-term simulations, which in turn requires the use of computationally efficient models that at the same time include a sufficient number of physical processes. Several Earth system models of intermediate complexity (EMICs) have been developed in recent years (Stocker et al. 1992; Prinn et al. 1999; Petouchov et al. 1999; Wiebe and Weaver 1999); see the review in Claussen et al. (2002) and a detailed description of different EMICs at http://www.pik-potsdam.de/data/emic/table_of_emics.pdf. According to Claussen et al. (2002), the key features of these

* Joint Institute for the Study of the Atmosphere and the Ocean Contribution Number 828

I.V. Kamenkovich (✉)
Department of Atmospheric Sciences,
University of Washington, Seattle, WA, USA
E-mail: Kamen@atmos.washington.edu

A.P. Sokolov · P.H. Stone
Center for Global Change Science,
Massachusetts Institute of Technology,
Cambridge, Massachusetts, USA

I.V. Kamenkovich
Joint Institute for the Study of the Atmosphere and the Oceans,
Box 354235, University of Washington,
Seattle, WA 98195-4235, USA

models are that they contain less detail than state-of-the-art coupled GCMs, and therefore have the advantage of greater computational efficiency, but include as many or more interacting components of the Earth system. The number of physical processes included in an EMIC, as well as the level of complexity of these processes, depends on the purpose of each particular study for which a model was developed.

In this work, we describe and illustrate the performance of a new climate model of intermediate complexity, which is the new climate component of the MIT Integrated Global System Model (IGSM) (Prinn et al. 1999). The full version of the IGSM also includes a model of atmospheric chemistry (Wang et al. 1998), a terrestrial ecosystems model ( Xiao et al. 1997), a natural emission model (Liu 1996), an ocean carbon model (Holian et al. 2001) and an economics model of anthropogenic emissions (Babiker et al. 2001). The fact that IGSM is specifically designed for studying climate change including assessment of different climate policies, imposes requirements on degree of complexity with which deferent processes should be treated in the model. For example, since the IGSM is forced by emissions, not concentrations, of different greenhouse gases (GHGs), an atmospheric model should be able to simulate transport of different chemical species. It also needs a radiation code that treats different GHGs separately. The climate model described here consists of the atmosphere, ocean and ice components. The atmospheric component (Sokolov and Stone 1998) was developed from the GISS General Circulation Model (GCM) (Hansen et al. 1983). It solves the zonally averaged primitive equations as an initial value problem and includes parameterizations of all the main physical processes usually included in GCMs. Therefore, it can simulate response of the zonal-mean atmospheric circulation to forcing associated with changes in concentrations of different GHGs and aerosols in a rather realistic way. This model coupled to a two-dimensional (zonal mean) diffusive ocean model (Sokolov and Stone 1998) has been used as a climate component of the IGSM in a number of climate change studies (Prinn et al. 1999; Reilly et al. 1999; Webster et al. 2001). In the climate model described here the zonal mean ocean model is replaced by a three-dimensional primitive-equation general circulation model (Kamenkovich et al. 2000) based on the MOM2 code (Pacanowski et al. 1995) with idealized geometry. The three-dimensional dynamically active ocean allows an explicit simulation of feedbacks associated with changes in the ocean circulation. At the same time, our coupled model is efficient enough computationally to be used in climate change studies that require carrying out multiple long-term climate simulations.

In most of the existing coupled atmosphere ocean general circulation models fluxes of heat, moisture and momentum through the atmosphere–ocean interface have to be adjusted to prevent drift of the climate system into an unrealistic state. Some of the recently developed most sophisticated atmosphere–ocean coupled models (Boville and Gent 1998; Gordon et al. 2000) are stable for multi-century integrations without such an adjustment. Systematic drift in temperature in the upper ocean in those models is significantly smaller than in the older generations of models (Manabe and Stouffer 1988). However, large drift in the salinity and deep-ocean temperature is still present even in those models (Boville and Gent 1998; Bryan 1998; Gordon et al. 2000), and at least in the former model the present-day climate simulation was stopped after 300 years because it was anticipated that the thermohaline circulation would eventually collapse (Boville and Gent 1998).

In spite of simplified representation of physical processes and/or dynamics in most EMICs, the degrees of freedom in these models exceed the number of adjustable parameters by several orders of magnitude (see Claussen et al. 2002). In other words, these models are not as easily tunable as conceptual models. As a result, while some of the models of intermediate complexity (Stocker et al. 1992; Petouchov et al. 2000; Wiebe and Weaver 1999) can simulate present-day climate without flux correction, others (Opsteegh et al. 1998; Goose et al. 2000) still require flux adjustment of some kind. In the model described here, a computational efficiency is achieved not by reduced complexity of the physical and dynamical processes but by decreased resolution, which does not make the model easily tunable. From this point of view, our model is similar to a GCM with coarse resolution and it too drifts without the use of flux adjustments. We devote a part of this study to the investigation of the general causes of the model's drift, which cannot be completely eliminated even in the many of more sophisticated models. Weaver and Hughes (1996) suggest that the mismatch between oceanic heat transport prior to coupling and that implied by atmosphere is the main cause for the drift in oceanic temperature. Systematic changes in the circulation can also strongly affect the temperature structure. To study these factors in detail, we perform a number of simulations without or with a partial flux adjustment.

The model's components and coupling procedure are presented in Sect. 2. We describe present-day climate simulations in Sect. 3, where we also analyze the origins of systematic drift in temperature and circulation in the model with no flux adjustment and the role of different flux adjustments in eliminating this drift. In Sect. 4, to evaluate the model's performance, we compare results of global warming simulations with our model with the results of similar simulations with comprehensive coupled AOGCMs. The summary and conclusions are presented in Sect. 5.

## 2 Description of the model

The atmosphere and ocean components were each spun up independently prior to coupling using observed surface fluxes and sea surface temperatures. The details of the model configurations, individual spin-ups and coupling procedures are outlined below.

### 2.1 Atmospheric component

The two-dimensional (zonally averaged) statistical–dynamical atmospheric model used in this study (Sokolov and Stone 1998) was developed from the GISS GCM (Hansen et al. 1983). The model solves the zonally averaged primitive equations in latitude-pressure coordinates. The model's grid is variable, but in standard version used here it contains 24 points in latitude, corresponding to a resolution of 7.826°, and 9 layers in the vertical. The model's numerics and most of the parameterizations of physical processes closely parallel those of the GISS GCM. The radiation code used in the model includes several greenhouse gases ($CO_2$, $CH_4$, $N_2O$, etc.) and different types of aerosols. The model also includes parameterizations of heat, moisture, and momentum transports by large-scale eddies (Stone and Yao 1987, 1990). The MIT 2D model has complete moisture and momentum cycles and reproduces most of the non-linear interactions and feedbacks simulated by atmospheric GCMs.

The 2D model, as well as the GISS GCM, allows four different types of surfaces in the same grid cell, namely open ocean, sea ice, land, and land ice. The surface characteristics as well as turbulent and radiative fluxes are calculated separately for each kind of surface, while the atmosphere above is assumed to be well-mixed zonally. The atmosphere model uses a realistic land/ocean ratio for each latitude. More detailed description of the model can be found in Sokolov and Stone (1998) and Prinn et al. (1999).

A thermodynamic ice model is used for representing sea ice. The model has two layers and computes ice concentration (the percentage of area covered by ice) and ice thickness. The ice model is used in all the experiments cited except one (DIRGMN), in which no ice formation is allowed.

As shown by Sokolov and Stone (1998), the atmospheric model reproduces the major features of the present-day zonally averaged atmospheric circulation reasonably well. Since the model is to be used for climate change predictions, it is noteworthy that the seasonal climate variations are also reproduced realistically. The model's sensitivity to an external forcing can be varied by changing the strength of cloud feedback (see Hansen et al. 1993; Sokolov and Stone 1998). The dependence of zonal-mean surface fluxes of heat and momentum on surface warming simulated by the 2D model is qualitatively similar to that shown by more sophisticated atmospheric GCMs (Sokolov and Stone 1998; Prinn et al. 1999). Vertical and latitudinal structure of the 2D model response is also consistent with the results of different GCMs. At the same time, the 2D model is much faster than a 3D GCM with similar latitudinal and vertical resolution.

The 2D model coupled to a simple Q-flux mixed layer/diffusive ocean model has been shown to reproduce, with an appropriate choice of the model's cloud feedback and effective diffusion coefficient, transient surface warming and sea level rise due to thermal expansion of the ocean as simulated by different coupled AOGCMs for 120–150 years (Sokolov and Stone 1998; Sokolov et al. 2001). Such a model cannot however represent feedbacks associated with changes in the ocean circulation. To take into account possible interactions between atmosphere and ocean circulation, the diffusive ocean model is replaced in this study by a 3D ocean GCM with simplified geometry.

### 2.2 Ocean component

The ocean component of the coupled model is based on the MOM2 code (Pacanowski et al. 1995) with idealized geometry. The model domain consists of two rectangular basins (Fig. 1): "Pacific", extending from 48°S to 60°N and "Atlantic" extending from 48°S to 72°N. The basins are connected by a channel ("ACC"), which extends from 48°S to 64°S; the model "Drake Passage" (between the Pacific and Atlantic) extends only from 52°S to 64°S. Note that the Weddell and Ross seas, where the Antarctic Bottom Water (AABW) is formed in the real ocean due to the sea ice formation, are not included in the model. Formation of AABW in a coarse resolution model is highly sensitive to values of the surface salinity

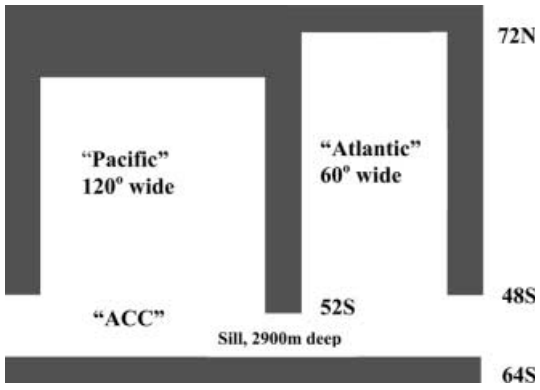


**Fig. 1.** Geometry of the ocean model

near the Antarctic coast and often requires adjusting salinity to unrealistically large values (England 1992). As a result, the AABW transport is difficult to control in a coupled simulation, which can lead to an additional source for a climate drift (Bryan 1998); on the other hand, in global warming experiments with coupled GCMs, this water mass has not played much role in determining the response of the THC. The mixed layer model described in the next section replaces the ocean GCM in the latitudes outside the 64°S–72°N latitude band. The Pacific basin is 120° wide and Atlantic is 60° wide.

The resolution in latitude is 4°; resolution in longitude varies from 1° near the meridional solid boundaries to 3.75° in the interior. Better resolution of the boundary currents has been shown to improve the simulated boundary currents and meridional heat transport in an ocean GCM (Kamenkovich et al. 2000). It also significantly improves the model's simulation of the mixing of tracers such as CFC11 and CFC12 into the deep ocean (V. Webb personal communication). This advantage would be offset if we used a realistic geometry, because the realistic orientation of boundary currents would require increased resolution in both horizontal directions and therefore a significantly larger number of grid points. The model has 15 layers in the vertical with thickness increasing downward from 50 m to 500 m. The ocean is 4500 m deep and the bottom is flat everywhere except in the Drake Passage, where there is a sill 2900 m deep. Although the topography in the North Atlantic has some affect on the vertical penetration of the NADW, models with no topography have been shown to reproduce global circulation and density structure reasonably well (Goodman 1998). The absence of topography, with the exception of the Drake Passage, is also consistent with the idealized geometry of the ocean basins. As a consequence of unrealistic ocean surface area, however, small adjustments in the surface heat and moisture fluxes are needed to make the model energy and salt conservative.

No-slip conditions for horizontal velocity are applied at the lateral walls. Free-slip conditions are used at the bottom, except in the ACC, where a bottom drag is applied. Boundary conditions for tracers are insulating at lateral walls and bottom. The standard version of our model incorporates the Gent-McWilliams (GM) parametrization scheme for tracer transports. For comparison purposes, both present-day climate and climate change simulations with horizontal diffusion (HD) were also carried out. Mixing coefficients are $5 \times 10^4$ and 0.01 $m^2\ s^{-1}$ for horizontal and vertical viscosity and $10^3$ and $5 \times 10^{-5}$ $m^2\ s^{-1}$ for horizontal and vertical tracer diffusivity. In the GM case, isopycnal diffusivity and isopycnal thickness diffusivity are $10^3$ $m^2\ s^{-1}$ each with no background horizontal diffusion.

The surface boundary conditions used to spin up the ocean model are taken from Jiang et al. (1999), who constructed the datasets using the data sources listed; see their study for a complete description of the datasets. The heat flux consists of two terms:

$$F_H = H_{obs} + C\rho\frac{(T_{obs} - T)}{\lambda}d_1 \quad (1)$$

The first term is the observed heat flux from dataset TS97 (Jiang et al. 1999; Trenberth 1998), an improved version of Trenberth and Solomon (1994). The second term on the right-hand side of Eq. (1) represents relaxation of model SST ($T$) to the observed SST ($T_{obs}$; Levitus and Boyer 1994). The restoring time scale $\lambda$ is 60 days, $d_1$ is the thickness of the upper layer (52 m), $C$ is the specific heat capacity, and $\rho$ is the density of the water. Note that the long-term average of this relaxation term would be zero if the model reproduced observed temperatures when forced by observed fluxes. This term therefore allows for correct representation of *both* heat fluxes and SST, whereas a simple relaxation of SST to its observed values leads to errors in the SST in regions of strong advection (Killworth et al. 2000). It is straightforward to show that condition Eq. (1) has the form of the Haney type boundary conditions linearized around SST (see the review in Paiva and Chassignet 2001).

The freshwater flux is specified and is based on precipitation and evaporation data from Baumgartner and Reichel (1975) and from Schmitt et al. (1989), river runoff data from Perry et al. (1996), and ice-calving data from Reeh (1994). Note that the surface freshwater fluxes do not include a conventional relaxation term (e.g., Gent et al. 1998). Although restoring of the surface salinity helps to keep its values close to the observed ones, it introduces an unrealistic dependence of freshwater fluxes on sea surface salinity and significant errors in the surface moisture fluxes (Jiang et al. 1999). Wind stress is taken from Trenberth et al. (1989).

We took basin zonal means of all observed quantities in the boundary conditions (data from Indo-Pacific are used for the model's Pacific). Heat and freshwater fluxes are re-balanced to ensure zero net flux through the ocean surface. The resulting forcing fields are shown in Fig. 2; the total flux $F_H$ (Fig. 2b) is shown for the GM run. The SST, heat fluxes, and wind stress have a seasonal cycle, while the freshwater flux is an annual mean.

We obtain two different equilibrium states, one with the use of GM and another with HD. The circulation has the form of a "conveyor belt" with water sinking in the North Atlantic (NA hereafter) and upwelling in the South Atlantic and Pacific oceans. SST is within 1.5 °C of the observed values.

## 2.3 Coupling procedure

Coupling takes place twice a day. The atmospheric model calculates 12-h means of values of the heat and fresh-water fluxes over the open ocean ($H_o$ and $F_o$), their derivatives with respect to SST ($\partial H_o/\partial T$ and $\partial F_o/\partial T$), the heat flux through the bottom of the ice ($H_1$) and the wind stress. These quantities are then linearly interpolated to the oceanic grid. Total heat and fresh-water fluxes for the ocean model are:

$$F_H = H_o(1-\gamma) + H_i\gamma + [\partial H_o/\partial T](T-\bar{T})(1-\gamma) \quad (2)$$

$$F_w = F_o(1-\gamma) + F_i\gamma + [\partial F_o/\partial T](T-\bar{T})(1-\gamma) \quad (3)$$

where $\gamma$ is the fractional ice area (ice concentration) and $F_i$ the fresh water flux due to ice melting/freezing. $T$ is SST at a given ocean point, and the overbar denotes its global zonal mean.

The last terms on the right-hand sides of the equations allow for zonal variations in surface flux forcing and account for the fact that the 2D atmospheric model computes heat and freshwater fluxes using zonal mean SST. It should be noted that strictly speaking $\partial H_o/\partial T$ and $\partial F_o/\partial T$ are not partial derivatives. Fluxes of sensible ($SH$) and latent ($LH$) heat are calculated in the atmospheric model by bulk formulas with turbulent exchange coefficients dependent on Richardson number (Sokolov and Stone 1995), and are nonlinear functions of SST. The near surface air temperature, however, adjusts to changes in surface fluxes relatively fast. Therefore, calculation of partial derivatives of $SH$ and $LH$ with respect to SST in a conventional way, under assumption of all other atmospheric variables being fixed, would lead to overestimation of $SH$ and $LH$ sensitivity to changes in SST, compare to estimates given in the literature (see, e.g., Rivin and Tziperman 1997; Frankignoul et al. 1998). $\partial SH/\partial T$ and $\partial LH/\partial T$ are instead calculated under the assumption that the exchange coefficients are fixed. That yields global averaged monthly mean values of $\partial SH/\partial T$ and $\partial LH/\partial T$ of 8–9 $Wm^{-2}\,K^{-1}$ and 17–19 $Wm^{-2}\,K^{-1}$, respectively. The values of $\partial SH/\partial T$ and $\partial LH/\partial T$ as well as their dependence on season and latitude are similar to those given by Rivin and Tziperman (1997). Possible changes in downward longwave radiation associated with changes in near surface air temperature and humidity are not taken into account. A partial derivative of upward longwave radiation is calculates as $4\sigma T^3$, where $\sigma$ a Stephan-Boltzman constant. Its global averaged monthly mean value is about 5.5 $Wm^{-2}\,K^{-1}$.

The last term in Eq. (3) represents variations in evaporation only, i.e., there are no longitudinal variations in precipitation in our model. To the extent that longitudinal variations in precipitation compensate longitudinal variations in evaporation, Eq. (3) can overestimate longitudinal variations in freshwater flux. Rivin and Tziperman (1997) however show that the sensitivity of evaporation to changes in SST is about three times as large as that of local precipitation, which suggests that the overestimation is not too large. Since the total ocean area in the ocean model is different from that used in the atmosphere, heat fluxes are adjusted so that the oceanic heat uptake per unit area is equal to the amount of heat lost/received by the atmosphere. The total moisture flux into the ocean is also made zero to conserve the total amount of salt stored in the ocean. We also do not take into account changes in run-off in Eq. (3). The zonal mean of the wind stress is used at each latitude. The atmospheric component also passes to the ocean model the amount of ice melted from above.

The ocean model, after being integrated twelve hours forced by these fluxes, supplies the atmosphere with a zonal mean of SST, sea ice thickness and sea-ice concentration. Values on the atmospheric grid are calculated as area-weighted means of corresponding values on the oceanic grid. Due to the different latitudinal extents of the two models (see Sect. 2.2), at the two southernmost and three northernmost points of the atmospheric grid, SST is calculated by a mixed-layer ocean model, which was adopted from the GISS GCM. Mixed layer depth is prescribed from observations as a function of time and latitude. In addition to the temperature of the mixed layer, the model also calculates the temperature of the seasonal thermocline and temperature at the annual maximum mixed layer depth (Russell et al. 1995). Sea-ice characteristics are calculated by a zonally averaged version of the sea-ice model described. In climate change simulations, heat mixing into the deep ocean at these points is parameterized by diffusion of the deviation of the mixed layer temperature from its present-day climate values (Sokolov and Stone 1998).

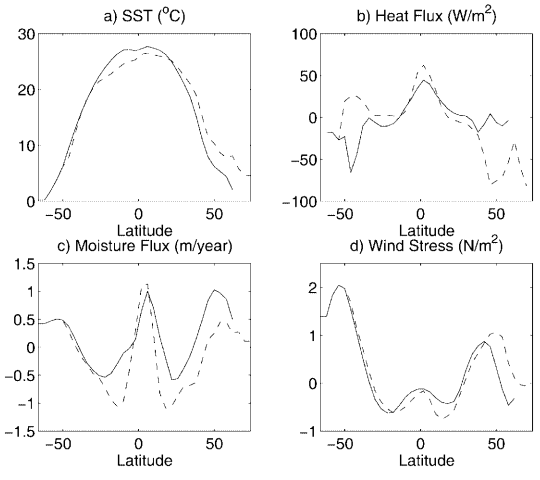


**Fig. 2a–d.** Surface boundary conditions used for the spin-up of the ocean component: Pacific basin (*solid line*) and Atlantic (*dashed line*). **a** SST (°C); **b** the total heat flux ($F_H$ in Eq. 1) into the ocean ($Wm^{-2}$) in the GM simulation (the HD result is similar); **c** freshwater flux into the ocean ($myr^{-1}$); **d** wind stress ($Nm^{-2}$)

We use here two different coupling procedures: one similar to flux adjustment (anomaly coupling) and one without any flux adjustment (direct coupling). Flux adjustments in the former method are calculated as differences between the values of heat, moisture and momentum fluxes used to spinup the ocean model (Sect. 2.2) and the corresponding values obtained in the simulation with the atmospheric model forced by observed SST and sea ice. In other words, in this mode the ocean model is forced by the *anomalies* in fluxes of the atmospheric model added to the corresponding climatologically based fluxes used in the ocean-only simulations. The anomalies per unit area are identical in both basins. In the anomaly coupling case the SST forcing the atmosphere is also adjusted by the difference between observed values and those diagnosed from the spin-up steady state of the ocean model. This adjustment however is very small and does not appreciably affect results. A similar coupling technique is implemented in simulations with the MPI AOGCM by Voss et al. (1998).

### 2.4 Asynchronous integration

We use an asynchronous integration (Bryan 1984) with different values of the ratio between time steps for tracer and momentum equations in the ocean model. Three values of this accelerating parameter were tested in current climate simulations prior to global-change experiments: unity (synchronous integration, 1 h for the tracer and momentum time steps), 12 (as12 case, 12 h and 1 h for tracer and momentum steps, respectively) and 192 (as192 case, 2 days and 15 min, respectively). Annual means of resulting dynamical fields agree well in all three cases. Monthly means of heat transport, however, show significant differences between the synchronous and the as192 cases. In contrast, results in the as12 case are very close to those from the synchronous integration. To illustrate this, we compare in Fig. 3 the monthly means of the meridional heat transports in the Atlantic (results for the Pacific basin are similar) from as192, as12 and the synchronous run for the anomaly-coupled model with the GM scheme. The as12 run is similarly successful in simulation observed SST (not shown).

We then test the applicability of the as12 technique again in an anomaly coupled global change experiment with $CO_2$ concentration increasing at the rate of 2% per year. Temporal changes in the circulation and temperature fields in this case are among the largest of all our experiments, and this case serves as another test of the asynchronous technique. The differences between the results of the as12 and synchronous calculations (not shown) are no larger than those shown in Fig. 3. Thus in what follows, we will employ asynchronous integration with accelerating factor 12. This allows us to increase the integration speed of the coupled model by a factor of 6.5. As a result, a 100 year coupled run with the ocean model employing the GM scheme takes less than 8 h on a single 500 MHz CPU of a Compaq Alpha Server DS20. In this configuration the atmospheric model takes about 40% of the total computational time.

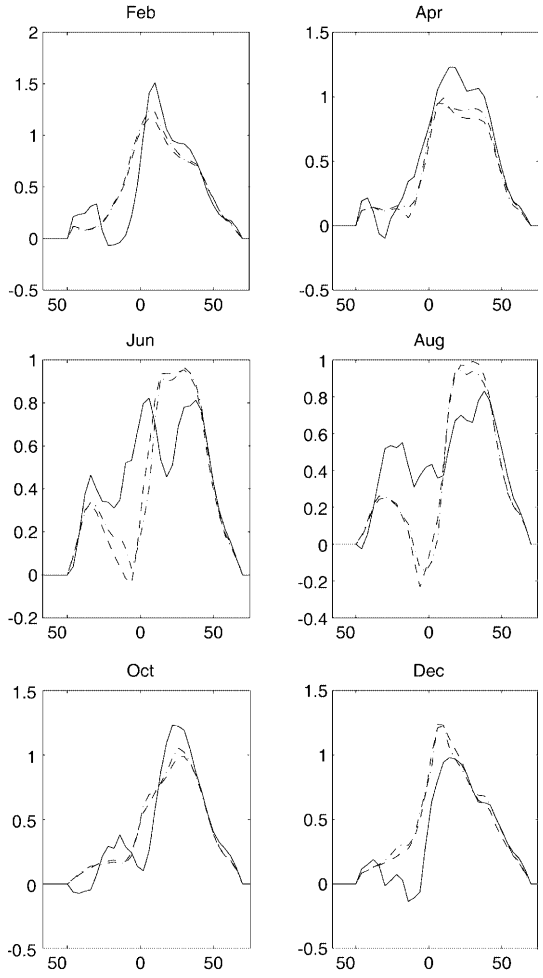


**Fig. 3.** Monthly mean meridional heat transports in the Atlantic for three different integration methods: as192 (*solid*), as12 (*dashed*), and synchronous (*dashed-dotted*). Corresponding month is given on the *top* of each panel. Units are petawatts

**Table 1.** Present-day climate simulations

| Name | Mixing scheme | Fluxes adjusted | | |
|---|---|---|---|---|
| | | Heat/SST | Moisture | Momentum |
| ANGM | GM | Yes | Yes | Yes |
| ANHD | HD | Yes | Yes | Yes |
| DIRGM | GM | No | No | No |
| DIRGMN (no sea ice) | GM | No | No | No |
| DIRHD | HD | No | No | No |
| WFWGM | GM | Yes | No | No |
| WIND | GM | Yes | Yes | No |

## 3 Present-day climate simulations

We now discuss the results of our coupled experiments. We base our analysis on annual mean, zonal average fields. The experiments are listed in Table 1.

### 3.1 Anomaly coupling: experiments ANHD and ANGM

Present-day climate simulations were performed with both the GM and HD mixing schemes (experiments ANGM and ANHD). In spite of the use of flux adjustment, the model undergoes some initial adjustment with global mean SST deviating by about 0.5 °C from its initial value (Fig. 4) and the NA meridional overturning increasing by less than 10% (Fig. 5). Such an adjustment usually occurs, when the oceanic and atmospheric components of a model were spun up separately (see, e.g., Mitchell et al. 1998). To ensure equilibrium the model was run for 200 years; the resulting zonal mean SST stays very close to observed values with deviations less than 1 °C. There is no sign of a system-

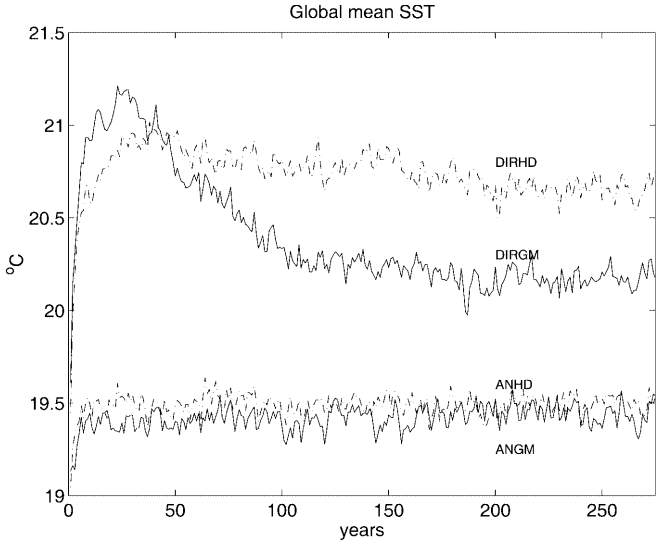


**Fig. 4.** Evolution in time of the global mean SST during the present-day climate simulations from four experiments: ANGM (*solid*), ANHD (*dashed-dotted*), DIRGM (*solid*), DIRHD (*dashed-dotted*). The curves are marked with the corresponding experiment name

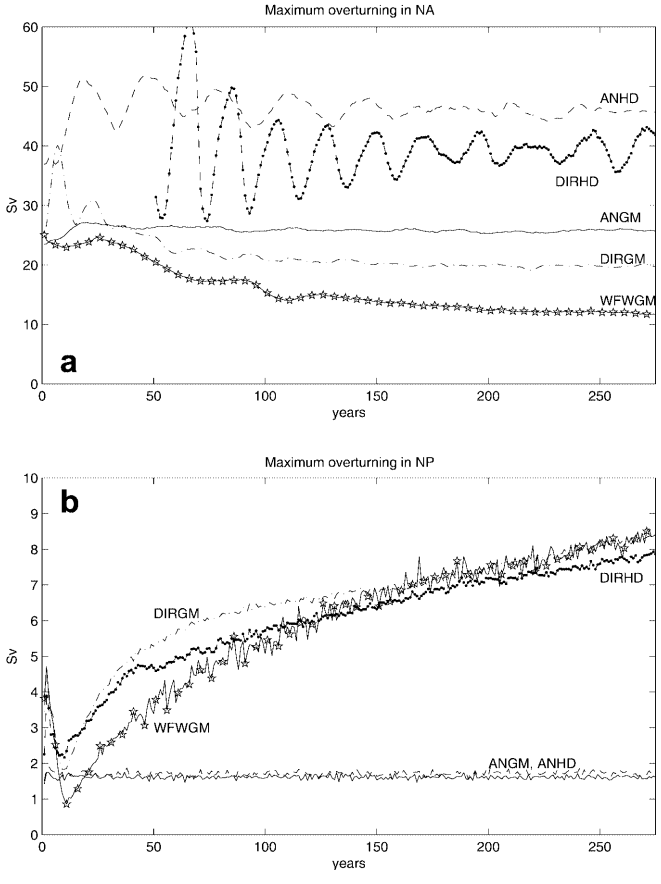


**Fig. 5a, b.** Evolution in time of the maximum (subsurface) meridional overturning during the present-day climate run for experiments: ANGM (*solid*), ANHD (*dashed*), DIRGM (*dashed-dotted*), DIRHD (*heavy dots*), WFWGM (*stars*). **a** North Atlantic (first 50 years of DIRHD not shown); **b** North Pacific

atic drift in the temperature or circulation after about 100 years of integration in either of the experiments. In the case of no flux adjustment, in contrast, there is a steady drift in the deep ocean temperature, and in the circulation in the Pacific basin; see the next section.

The simulated salinity is shown as an average over the upper 500 m in Fig. 6, which is a more appropriate measure of the contribution of salt in the upper layers to meridional pressure gradients than surface values; the deviations from the Levitus values at the surface are similar. The upper model ocean is systematically fresher than the observations with the difference in the Southern Hemisphere being the largest. This is a consequence of our choice not to use restoring to surface salinity during the spin-up of the ocean model. Such restoring introduces an unrealistic dependence of moisture fluxes on surface salinity and produces unrealistic surface moisture fluxes (Jiang et al. 1999). The agreement with observations is better in ANHD. The errors in surface salinity are similar in magnitude to those shown in Fig. 6.

The differences in results between experiments with GM and HD have been documented before in a number of studies (e.g., Duffy et al. 1997; Jiang et al. 1999; Kamenkovich et al. 2000). The meridional overturning has a much more realistic strength in ANGM than it does in ANHD (26 Sv versus 46 Sv; see Fig. 7). Deep-ocean temperature is also more realistic in ANGM and is about 2 °C colder than in ANHD, and the vertical temperature contrast is larger. The sharper vertical temperature contrast in ANGM compensates for the weaker circulation, so that heat transports in the two cases are close to each other (Jiang et al. 1999; Kamenkovich et al. 2000).

Two important differences are also observed in the ACC region in agreement with the results of

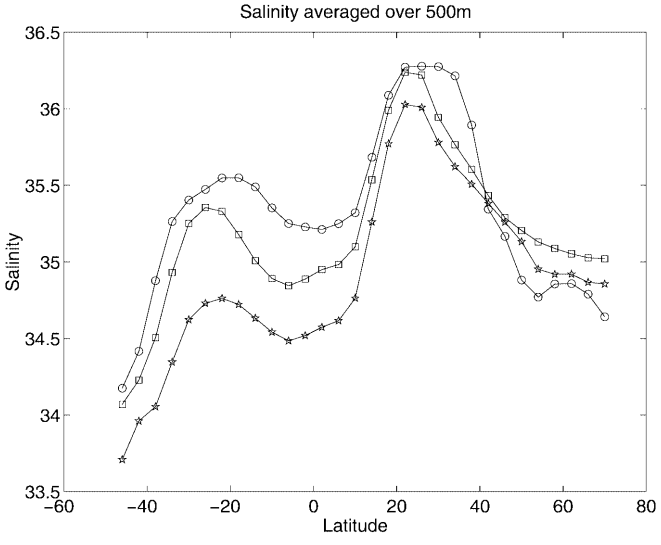


**Fig. 6.** Salinity in the Atlantic basin averaged over the upper 500 m: ANGM (*stars*), ANHD (*squares*), and Levitus values (*circles*)

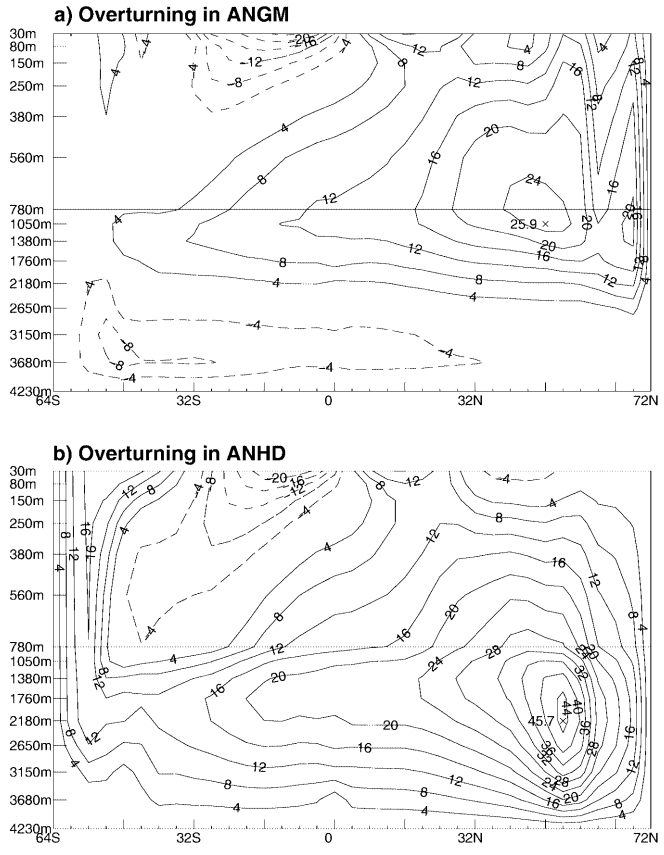


**Fig. 7a, b.** Annual mean of the global meridional overturning stream function (Sv). **a** ANGM (with eddy induced transport velocities added); **b** ANHD. The contour interval is 4 Sv

Danabasoglu and McWilliams (1995). Firstly, the deep convection, which is active in this region in ANHD, is eliminated in ANGM. Secondly, in ANHD, there is a wind-driven Deacon cell, which has a transport of 18 Sv at its maximum near the surface at 52°S and extends to 1000 m depth. The Deacon cell is partially cancelled by eddy induced transport velocities in ANGM, so that its effective transport is less than 6 Sv. This reduction in the convection and vertical advection in the Southern Ocean results in weaker vertical mixing of tracers in ANGM, as first suggested by McDougall et al. (1996).

The main features of the atmospheric circulation produced in both cases are very similar to each other and to those obtained in a present-day climate simulation with the atmospheric model alone (Sokolov and Stone 1998). This is not surprising, since, as mentioned, the simulated zonal-mean SST in both cases is very close to its observed values.

In both the ANGM and ANHD simulations, sea-ice formation takes place only in the points treated by a mixed layer ocean model, while no sea ice is formed in the 3D ocean model domain. As a result, the simulated latitudinal extent of the sea ice is somewhat smaller than both the observed, and that obtained in a present-day climate simulation with the atmospheric model coupled to a mixed layer ocean model.

## 3.2 Direct coupling: causes for the climate drift. Experiments DIRGM and DIRHD

Similar to the anomaly coupled experiments, we conduct directly coupled experiments (no flux adjustment) with the two mixing schemes: the GM scheme (experiment DIRGM) and the HD scheme (experiment DIRHD). Due to differences in the surface fluxes produced by the atmospheric component and those used for the spin-up of the oceanic component, the coupled model with either mixing scheme undergoes a significant adjustment during the initial spin-up.

### *3.2.1 Surface response*

The globally averaged SST reaches a quasi-equilibrium state after the first 150 years of integration (Fig. 4), with subsequent variations smaller than 0.2 °C.The value on which global SST settles by the year 275 is, however, larger than that in the uncoupled state by about 1.2 °C in DIRGM and by about 1.7 °C in DIRHD. This warming of the entire ocean surface in the directly coupled simulations is partly explained by the initial mismatch between oceanic heat transport and that implied by the atmosphere prior to coupling. In addition, unrealistically small ice cover in the NH of the ocean model leads to significant warming in high latitudes of NH; the warming then spreads southward reaching the SH as the maps of the air temperature demonstrate (not shown).

In Fig. 8a, we plot the difference between the heat flux into the ocean in the atmosphere-only run and the divergence of the heat transport per meter of longitude (in $Wm^{-2}$) in two ocean-only (spin-up) experiments. Note that the SST rises at the locations where the heat flux from the uncoupled atmosphere is larger than the divergence of the heat transport in an uncoupled ocean; see e.g., warming near the equator (Fig. 8b). Due to the large thermal inertia of the ocean, its heat transport does not change during the initial stage of coupling, and is not balanced by the heat flux from the atmosphere (Fig. 8a). As a result, surface temperature generally rises, causing the air-sea fluxes of heat into the ocean to decrease until they match the convergence of the oceanic heat transport, and equilibrium can be achieved. This leads to the warming of the upper ocean layers and the overlying atmosphere. The largest increase in SST is centered at 50°N, where the mismatch between atmospheric flux into the ocean and divergence of oceanic heat transport is the largest and surface warming is reinforced by the resulting increase in the cloud cover (not shown). At 20°N and 30°S the situation is the opposite with now the atmospheric heat flux initially out of the ocean, whereas oceanic heat transport is convergent at these locations. The expected local cooling is however masked by the overall warming of the atmosphere in the NH, described above. As a result, the SST changes near 20°N show only a local minimum with no

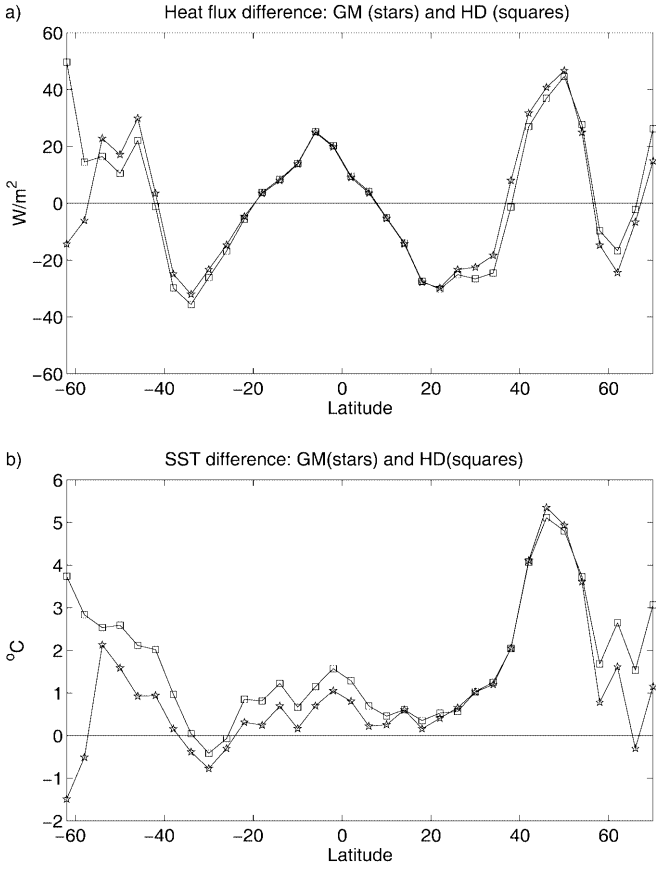


**Fig. 8.** **a** Difference between the heat flux through the lower boundary of the ocean fraction of the atmosphere model in its steady, uncoupled state and the divergence of the vertically and zonally integrated oceanic heat transport per m of longitude. Two uncoupled steady states: GM (*stars*) and HD (*squares*). Units: $Wm^{-2}$. **b** Deviations of SST simulated in the directly coupled present-day climate runs from Levitus SST: DIRGM (*stars*), DIRHD (*squares*)

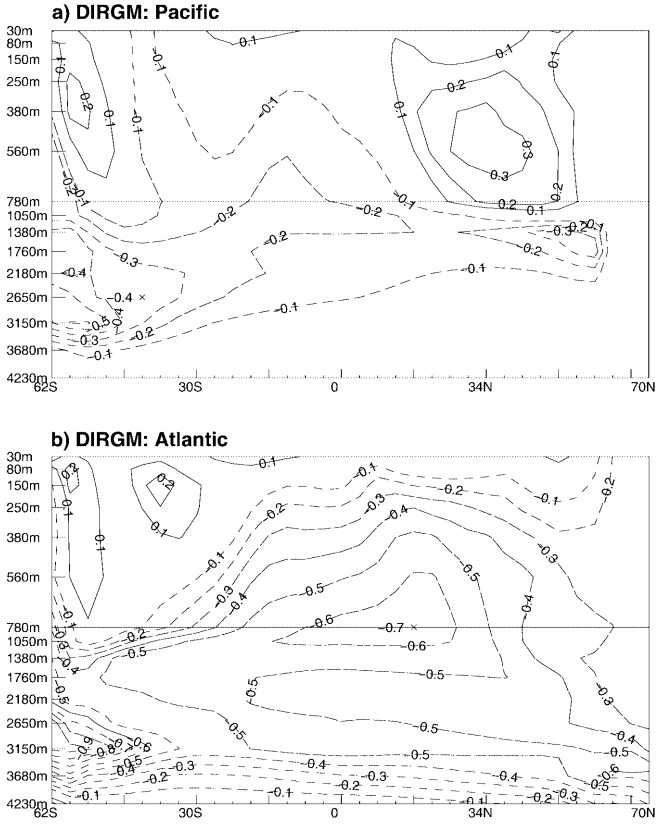


**Fig. 9a, b.** Drift in the zonally averaged ocean temperature, computed as a difference between its values averaged over years 266–275 and 201–205. Contour interval is 0.1 °C. Experiment DIRGM. **a** Pacific; **b** Atlantic

cooling, and the cooling at 30°S is less than 1 °C (Fig. 8b).

Deviations in the SST at the two southernmost points of the oceanic domain (Fig. 8b) have an additional impact on sea-ice distribution in the model. The oceanic poleward heat transport in this area prior to coupling is larger in the HD case than in the GM case, mainly because of the unrealistic diffusive heat transport in the former case. The heat convergence in the ocean in the coupled state is then unbalanced by a smaller heat loss to the atmosphere (Fig. 8a); the temperature rises as a result. This rise in the water temperature above climate values makes freezing impossible and the sea ice is absent in DIRHD. The extensive convection, which removes water from the cold polar air, further contributes to the absence of the sea ice in the model (Wiebe and Weaver 1999).

The situation is opposite in the GM case, with the heat transport convergence at 62°S being smaller in amplitude than the cooling at the surface (Fig. 8a). As a result, the SST is colder than its observed values (Fig. 8b) and a significant amount of ice is formed in the DIRGM experiment at the southernmost oceanic grid point at 62°S. The ice thickness is below 3 m everywhere in the domain with the exception of limited areas. The ice thickness in those regions reaches 10 m by the year 200 and then begins to decrease. The zonally averaged ice mass at 62°S does not reach an equilibrium value, with the annual maximum value (reached in October) decreasing from 4500 kg $m^{-2}$ in year 200 to 2800 kg $m^{-2}$ in year 275. The annual minimum (reached in March) also decreases from 3000 kg $m^{-2}$ to 1200 kg $m^{-2}$. Further integration does not lead to stabilization of the ice mass.

### *3.2.2 Deep temperature drift. Experiments DIRGMN and WFWGM*

The deep ocean temperatures continue to drift in DIRHD and DIRGM and the global mean oceanic surface heat flux fluctuates around –1 W $m^{-2}$, indicating the overall cooling of the ocean. The systematic drift below the surface is the largest in DIRGM, where the deep temperature continues to change throughout the last 75 years of integration, with noticeable systematic cooling of most of the ocean and some warming at mid-latitudes in the Northern Pacific (Fig. 9). In addition, the circulation is also changing, with sinking in the NP slowly

increasing (Fig. 5b) together with the systematic increase in North Pacific (NP henceforth) surface salinity characteristic of many models with climate drift (Manabe and Stouffer 1988; Stocker et al. 1992). This indicates a transition to a circulation pattern different from a "conveyor belt", with active sinking in both the NA and NP. Although the rate of the temperature drift decreases with time, the drift of the circulation toward an unrealistic state of "symmetric sinking" dissuaded us from carrying the experiment for longer times. It is noteworthy that the NA sinking exhibits significantly larger interannual variability in DIRHD than it does in DIRGM (Fig. 5a). The difference is smaller but still well pronounced in both the present-day climate and climate change anomaly-coupled runs (Fig. 5a and the next section).

As discussed in the introduction, the drift in deep ocean temperature is common for many coupled models. The drift is in part due to the fact that it takes a long time for the bulk of the ocean to fully adjust to the change in SST caused by the mismatch in heat transports of the two component models. In addition, changes in the circulation and formation of ice in DIRGM can each be a factor in causing systematic temperature changes.

To separate the causes for the temperature drift, we carried out additional experiments with the GM scheme. To investigate the role of sea ice in our model, we conduct experiment DIRGMN, in which we allow no sea-ice formation in the ocean component, but it is otherwise identical to DIRGM. We remind the reader that almost no ice was formed in the ocean-only simulations. The ocean temperature in DIRGMN is not allowed to decrease below the freezing point. No changes were made in ocean points treated by the mixed layer model. Comparison of the results of DIRGM and DIRGMN simulations (Fig. 10) shows that the decrease in the deep ocean temperature in high and middle latitudes of the Southern Hemisphere is noticeably stronger when sea ice is formed. The drift in this region is, therefore, largely explained by the intensive production of the dense bottom water in DIRGM, triggered by the salt rejection during ice formation. This cold and salty water then sinks to the bottom and propagates northward. The process is similar in nature to that in the NCAR climate model (CSM) reported by Bryan (1998), who identifies an excessive freshwater transport by their ice model as a primary cause for the change. The surface of the Southern Ocean is warmer when ice is formed largely because of the insulating effect of the ice sheet on the underlying waters.

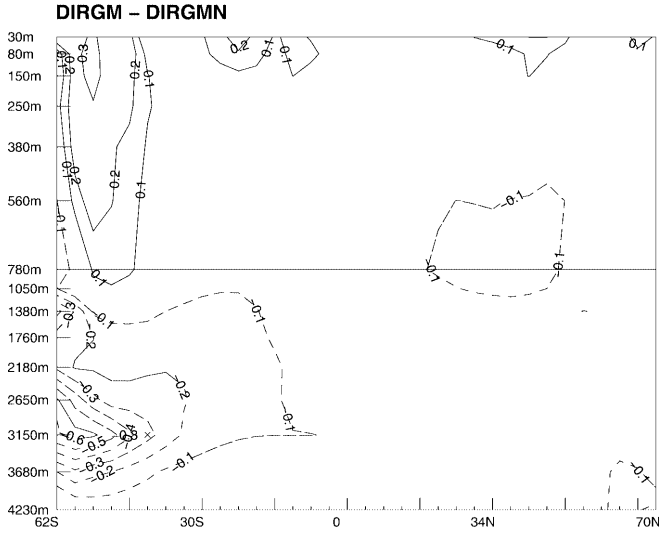


**Fig. 10.** Difference between the global zonal mean of the temperature drift (as defined in Fig. 9) in DIRGM and DIRGMN (no ice)

We next carried out an experiment WIND (not shown), in which only the momentum flux is coupled directly, whereas fluxes of heat and moisture are coupled through anomalies. After an initial adjustment related mostly to changes in the transport of the ACC, the deep temperature does not exhibit a systematic drift. The strength of the vertical overturning in either basin is steady and not very different from the one in the ANGM. The interannual variability in the circulation strength is however amplified in WIND and is now similar to that in the DIRGM. We therefore conclude that the method of coupling of the momentum fluxes does not affect systematic deviations in the deep temperature.

In the third additional experiment, WFWGM, the moisture and momentum fluxes are coupled directly, whereas the heat flux is coupled through anomalies. No sea ice develops in the ocean model. The drift in the circulation is now present in *both* basins; in addition to intensifying sinking in the NP, also present in DIRGM, the sinking in the NA weakens substantially. At the end of the run the circulation is already in a state different from the "conveyor belt": the sinking rate in the NA is only 12 Sv at the end of the experiment; with the NP sinking rate equal to 8.5 Sv (Fig. 5a, b). In contrast, the NA sinking is robust in DIRGM (Fig. 5a).

The fact that the NA overturning decreases in WFWGM, in which only the heat fluxes are adjusted, whereas it is stable in DIRGM, suggests that the adjustments in the heat flux have a destabilizing effect on the meridional overturning in the NA. A possible explanation is related to the inter-basin exchanges of moisture. As Fig. 11a, b shows for WFWGM, the freshwater flux into the NA is larger than the one into NP; this asymmetry acts to weaken the "conveyor". In contrast, the NA freshwater flux is smaller than the NP flux in DIRGM and ANGM. This difference can only be explained by the NA in WFWGM being colder than NP, which results in the freshwater flux being from NP into NA (see Eq. 3); NA is warmer than NP in both ANGM and DIRGM. The parametrization of this flux used in the model can only represent zonal re-distribution of evaporative freshwater flux in an idealized manner (see Sect. 2.3); a three-dimensional atmosphere model would be needed for a more accurate representation of zonal

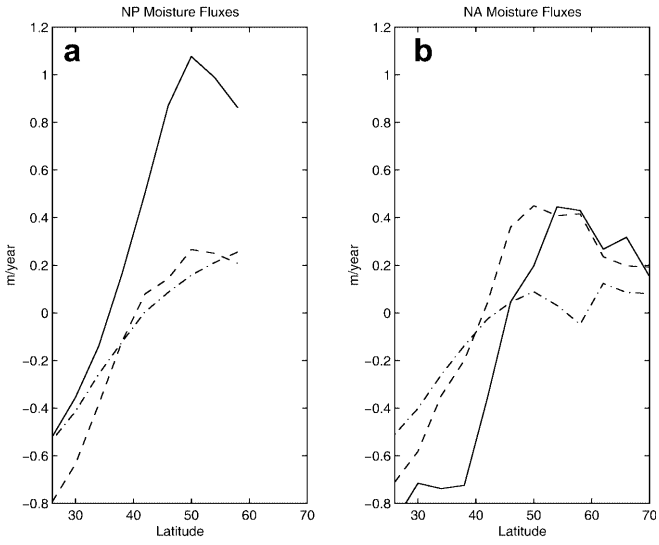


**Fig. 11a, b.** Zonally averaged, annual mean freshwater fluxes into the ocean ($myr^{-1}$): **a** North Pacific and **b** North Atlantic oceans: ANGM (*solid*), DIRGM (*dashed-dotted*), and WFWGM (*dashed*). Mid to high latitudes of the Northern Hemisphere only

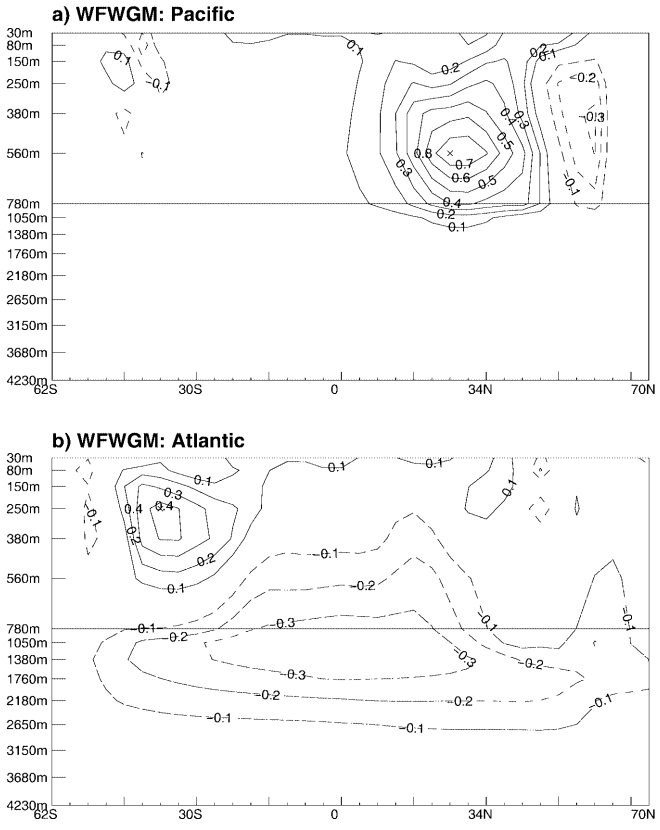


**Fig. 12a, b.** As in Fig. 9, but for the experiment WFWGM

moisture transfers. This cooling of NA in WFWGM is caused by the heat flux adjustments. We remind the reader that the flux adjustments are calculated as the difference between air-sea fluxes in the ocean-only climate and a zonally uniform flux in the atmosphere-only climate. The heat flux adjustments, act to lower SST in NA with respect to NP. This cooling induces a transfer of moisture from NP into NA, which slows the NA sinking. The decrease in the overturning strength leads to the drop in the meridional heat and salt transports and further cooling and freshening of the NA. The effect of the freshening of the surface waters in NA wins over that of the cooling and the sinking continues to weaken.

It is noteworthy that in WIND, where in addition to heat fluxes freshwater fluxes are also adjusted, the drift in the circulation is absent in either basin. We can therefore conclude that the adjustments in the freshwater fluxes act to *maintain* the "conveyor belt" in the model. In particular, a large freshwater flux into the NP (Fig. 11a) prevents relatively cold surface waters there from sinking. In contrast, smaller amplitudes of the directly coupled freshwater flux through the surface of NP in DIRGM and WFWGM (Fig. 11a) cause the intensification of sinking in the region. Increased circulation results in the increase in the associated northward salt transport, which acts to further increase salinity and thus enhance the sinking.

The overall cooling of the ocean in DIRGM is markedly reduced in WFWGM in both basins. We remind the reader, that in the latter case only heat fluxes are adjusted, but the drift in the circulation is present in both basins. We therefore conclude that the strong cooling in DIRGM is mainly caused by the mismatching heat transports in the uncoupled states of atmospheric and oceanic model components. Thus in the Pacific (Fig. 12a), the cooling is practically absent in WFWGM, while the drift in the circulation in that basin is similar between DIRGM and WFWGM. The only remaining temperature drift in the Pacific in WFWGM is warming of the upper NP, and is clearly related to the drift in the circulation, since the intensifying NP sinking acts to increase the subsurface temperature in the basin by bringing down the warm surface waters. The pattern of the resulting warming of the upper kilometer of the ocean in the mid-latitudes of the NP basin is very similar between DIRGM and WFWGM, although the warming is almost twice as strong in WFWGM; compare Figs. 9a and 12a. In the Atlantic, the NA overturning acts to warm the deep ocean by bringing warmer surface waters down; the weakening of the NADW overturning in WFWGM therefore must act to cool the ocean below the thermocline; see Manabe and Stouffer (1988) for their comparison of the equilibria with and without the NADW overturning. The Atlantic cooling in WFWGM (Fig. 12b) is then mostly caused by the weakening NADW overturning, since heat fluxes are adjusted here. Since the NADW overturning is stable in DIRGM, the cooling of the Atlantic in that run is caused by the mismatch between heat transports in two model components.

## 4 Global warming simulations

To evaluate the model's response to external forcing, we performed several anomaly coupled simulations with

**Table 2.** Climate change simulations

| Name | Model's sensitivity, K | $CO_2$ increase | |
|---|---|---|---|
| | | Rate per year | Length, years |
| 1/75 | 2.5 | 1% | 75 |
| 1/75H | 4.5 | 1% | 75 |
| 1/150 | 2.5 | 1% | 150 |
| 2/75 | 2.5 | 2% | 75 |

increasing atmospheric $CO_2$ concentration. The design of these experiments is very similar to that in a number of the previously published studies cited. We therefore present here our results with the sole purpose of evaluating general performance of our model compared to other existing models of, in some cases, greater degree of sophistication. In this section, we briefly present results of four simulations with the GM parametrization. These simulations are summarized in Table 2. In three of them (1/75, 2/75 and 1/75H) the atmospheric $CO_2$ concentration increases at the rate of either 1% or 2% per year (compounded) for 75 years; it is kept constant after that, and the model is integrated for 600 years more. In the fourth experiment (1/150) atmospheric $CO_2$ increases at the rate of 1% per year for 150 years. Three simulations were carried out with the standard version of the atmospheric model, while in simulation 1/75H the sensitivity of the atmospheric model was increased through additional cloud feedback (see Sect. 2.2). The model's sensitivity, defined as the equilibrium surface warming which would be caused by the $CO_2$ doubling in a simulation with the atmospheric model coupled to a mixed layer ocean model, was calculated to be about 2.5 °C in the standard model and 4.5 °C in 1/75H.

The temperature response shows the usual dependence on the rate of $CO_2$ increase (Schmittner and Stocker 1999; Stouffer and Manabe 1999), namely the warming is slightly larger for a lower rate of $CO_2$ increase (Fig. 13a) for a given total increase in $CO_2$. Namely, in our simulations, the surface temperature rises by 1.4 °C and 1.6 °C at the time of $CO_2$ doubling and by 3.6 °C and 4.1 °C at the time of $CO_2$ quadrupling for 2% and 1% per year rates correspondingly. Warming of the deep ocean shows a stronger dependence. At the same time, NA sinking (Fig. 13b) slows down from about 25.5 Sv at the beginning of the experiments to about 21 Sv by the time of $CO_2$ doubling and to 15.5 Sv at the time of $CO_2$ quadrupling *regardless* of the rate. In contrast, in simulations with the GFDL AOGCM (Stouffer and Manabe 1999) the reduction in the strength of the THC caused by doubling of $CO_2$ increases with decrease in the rate of $CO_2$ change.

As a whole, changes in the NA meridional overturning in the simulations with the standard version of our model are smaller than those produced by the GFDL AOGCM (Manabe and Stouffer 1994; Stouffer and Manabe 1999), but are similar to those obtained with the HadCM3 AOGCM (Wood et al. 1999) and with ECHAM3/LSG AOGCM (Mikolajewicz and Voss

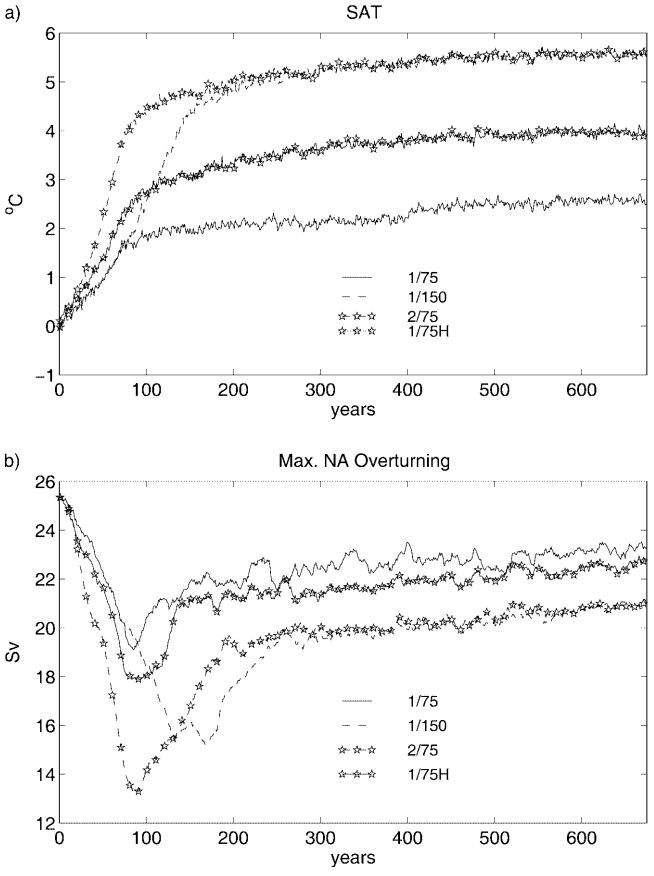


**Fig. 13.** Evolution in time of the: **a** global mean SAT, given in the form of changes from the initial values for easier comparison; **b** maximum (subsurface) meridional overturning in global warming simulations: 1/75 (*solid*), 1/150 (*dashed*), 1/75H (*solid with stars*), 2/75 (*dashed with stars*); see Table 2

2000). In simulations with both the HadCM3 and ECHAM3/LSG, as well as with our model (1/150 and 2/75), quadrupling of $CO_2$ leads to a rather moderate decrease in the strength of the THC, of about 7, 12, 10 and 10 Sv at the time of $CO_2$ quadrupling respectively, followed by a recovery which starts 10–15 years after $CO_2$ is fixed. In the simulation with the GFDL AOGCM, in contrast, the THC collapses completely. The climate sensitivity of the GFDL AOGCM is 4.5 °C (Stouffer and Manabe 1999) and is higher than the sensitivities of the other models mentioned. Our results, however, show only a weak dependency of the rate of decrease of the strength of THC on model sensitivity. In particular, the difference in the strength of the meridional overturning between simulations 1/75 and 1/75H does not exceed 2 Sv (Fig. 13b).

An interesting feature of the 1/150 simulation is that the thermohaline circulation stops slowing down after 130 years of integration despite the continuing increase in $CO_2$ concentration. In an analogous simulation by Wiebe and Weaver (1999), the circulation starts to recover after 90 years of integration, that is some 50 years before $CO_2$ concentration quadruples. In 2/75, NA sinking continues to slow down after $CO_2$ is fixed but

recovers faster than in the simulation 1/150. Such a dependence of the recovery of the THC on the rate of $CO_2$ increase is in agreement with results of Stouffer and Manabe (1999).

## 5 Summary and discussion

We have introduced a climate model of intermediate complexity, which consists of a 2D (zonally averaged) statistical–dynamical atmospheric model coupled to a 3D ocean model with a simplified geometry. The model is sufficiently efficient computationally to allow a large number of multiple-century integrations; and at the same time uses parameterizations of physical processes and dynamics similar to those used in GCMs. The efficiency results in part from the asynchronous integration of the oceanic momentum and tracer equations. This is feasible, i.e., the errors are small, as long as the ratio between time steps is not too large (12 in our case). It would be interesting to test this result in a more realistic ocean model. The use of the flux-adjustment technique prevents the model from systematically drifting and keeps the surface temperature close to the observed values. The thermohaline circulation in the present-day climate simulations remains steady with the maximum magnitude of the overturning 26 Sv and 44 Sv in the GM and HD cases respectively.

The use of rather sophisticated parameterizations together with a coarse spatial resolution makes the model less tunable than most of EMICs. It is not surprising that our directly coupled model shows systematic deviations in the temperature field both at and below the surface. Such a drift is characteristic for most contemporary coupled AOGCMs. Initial disagreement between the heat flux into the ocean produced by the atmospheric model in its uncoupled steady state and the divergence of the oceanic heat transport in the oceanic uncoupled state leads to the changes in the temperature of the upper ocean. The biggest differences with the observed values are found at the places where the mismatch is at its maximum. In particular, in the 40°N to 50°N latitude belt the *convergence* of the oceanic heat transport coupled with the atmospheric heat flux *into* the ocean leads to anomalous warming of the ocean surface. Increased humidity of the overlying atmosphere reinforces these positive anomalies in the surface temperature. This positive feedback helps the surface achieve a new steady state with distorted surface climate. Another source of the drift in the surface temperature is the warming originating from the high latitudes in the NH and caused by the decreasing ice cover.

The temperature in the subsurface layers of the directly coupled model, in contrast, exhibits a systematic drift throughout the experiments. The largest portion of this drift is explained by the mismatch in the heat fluxes of the atmospheric and oceanic models, as was originally suggested by Weaver and Hughes (1996). We demonstrate this by carrying out an experiment, in which only the heat flux is adjusted, while moisture and momentum fluxes are coupled directly. The resulting drift is significantly reduced. The remaining portion can be attributed to drift in the circulation, caused by the changing freshwater fluxes and the excessive formation of sea ice at the Antarctic coast. It is noteworthy that the circulation deviates from the "conveyor belt" even more strongly in this experiment than in the simulations with all fluxes adjusted and without flux adjustment: the NA sinking nearly halves during the simulation. We conclude that the adjustments of heat and freshwater fluxes tend to have opposite competing effects on the NA overturning in our model. The heat flux adjustments apparently act to weaken the circulation in the NA, whereas the freshwater flux adjustments sustain the "conveyor belt".

The model's response to an increase in the atmospheric $CO_2$ concentration is similar to that in analogous simulations with more detailed coupled AOGCMs. For example, our simulations show dependence of surface warming on the rate of $CO_2$ increase that is similar to that found in several coupled AOGCMs. Changes in the strength of the thermohaline circulation also agree with results of recently developed AOGCMs. Interestingly enough, our model shows almost no dependence of the rate of the weakening of the THC on the model's climate sensitivity.

Thus, the results presented show that the climate model described, in spite of much simplification, successfully reproduces a number of major features of the present-day circulation of the oceans and its evolution in global warming scenarios as simulated by more sophisticated coupled atmosphere ocean GCMs. The model's computational efficiency makes it especially suitable for studies requiring a significant number of long-term simulations. Another attractive feature of the model is the explicit representation of the zonal mean circulation in the atmosphere, which makes the model suitable for studies of the variations in the atmosphere's dynamics.

**Acknowledgements** We are grateful for the helpful suggestions by two anonymous reviewers. Igor Kamenkovich was supported by the Joint Institute for the Study of the Atmosphere and Ocean (JISAO) under NOAA Cooperative Agreement NA67RJ0155, Contribution 828. This research was supported in part by MIT's Joint Program on the Science and Policy of Global Change, and in part by the US Department of Energy's Office of Biological and Environmental Research under Grant DE-FG02-93ER61677 to MIT.

## References

Babiker MH, Reilly JM, Mayer M, Eckaus RS, Sue Wing I, Hyman RC (2001) The MIT emissions prediction and policy analysis (EPPA) model: revisions, sensitivities, and comparisons of results. MIT Joint Program on the Science and Policy of Global Change. Rep 71, MIT, USA

Baumgartner A, Reichel E (1975) The world water balance. Elsevier, Amsterdam, pp 179

Boville BA, Gent PR (1998) The NCAR climate system model. Version one. J Clim 11: 1115–1130

Bryan K (1984) Accelerating the convergence to equilibrium of ocean–climate models. J Phys Oceanogr 2: 510–514

Bryan F (1998) Climate drift in a multicentury integration of the NCAR Climate System Model. J Clim 11: 1455–1471

Claussen M, Mysak LA, Weaver AJ, Crucifix M, Fichefet T, Loutre M-F, Weber SL, Alcamo J, Alexeev VA, Berger A, Calov R, Ganapolski A, Goose H, Lohman G, Lunkeit F, Mokhov II, Petoukhov V, Stone P, Wang Z (2002) Earth system models of intermediate complexity: clothing the gap in the spectrum of climate system models. Clim Dyn 18: 579–586

Danabasoglu G, McWilliams JC (1995) Sensitivity of the global thermohaline circulation to parameterizations of mesoscale tracer transports. J Clim 8: 2967–2986

Duffy PB, Caldiera K, Selvaggi J, Hoffert MI (1997) Effects of subgrid scale mixing parameterizations on simulated distributions of natural C14, temperature, and salinity in a three-dimensional ocean general circulation model. J Phys Oceanogr 27: 498–523

England M (1992) On the formation of Antarctic Intermediate and Bottom Water in ocean general circulation models. J Phys Oceanogr 22: 918–926

Frankignoul C, Czaja A, L'Heveder B (1998) Air-sea feedback in the North Atlantic and surface boundary conditions for ocean models. J Clim 11: 2310–2324

Gent PR, Bryan FO, Danabasoglu G, Doney SC, Holland WR, Large WG, McWilliams JC (1998) The NCAR climate model global ocean component. J Clim 11: 1287–1306

Gordon C, Cooper C, Senior CA, Banks H, Gregory JM, Johns TC, Mitchell JFB, Wood RA (2000) The simulation of SST, sea-ice extents and ocean heat transports in a version of the Hadley Centre coupled model without flux adjustments. Clim Dyn 16: 147–168

Goodman P (1998) The role of North Atlantic deep water formation in an OGCM's ventilation and thermohaline circulation. J Phys Oceanogr 28: 1759–1785

Goose H, Selten FM, Haarsma RJ, Opsteegh JD (2000) Decadal variability in high northern latitudes as simulated by an intermediate-complexity climate model. Ann Glaciol (in press)

Hansen J, Russell G, Rind D, Stone P, Lacis A, Lebedeff S, Ruedy R, Travis L (1983) Efficient three dimensional global models for climate studies: Models I and II. Mon Weather Rev 111: 609–662

Hansen J, Lacis A, Ruedy R, Sato M, Wilson H (1993) How sensitive is world's climate? Nat Geogr Res Expl 9: 142–158

Holian G, Sokolov AP, Prinn RG (2001) Uncertainty in atmospheric $CO_2$ predictions from a parametric uncertainty analysis of a global ocean carbon cycle model. MIT Joint Program on the Science and Policy of Global Change. Rep 80, MIT, USA

Jiang S, Stone PH, Malanotte-Rizzoli P (1999) An assesment of the GFDL ocean model with coarse resolution. Part I: annual-mean climatology. J Geophy Res 104: 25,623–25,646

Kamenkovich I, Marotzke J, Stone P (2000) Factors affecting meridional heat transport in ocean general circulation models. J Phys Oceanogr 30: 175–194

Killworth PD, Smeed DA, Nurser AJG (2000) The effects on ocean models of relaxation toward observations at the surface. J Phys Oceanogr 30: 160–174

Levitus S, Boyer TP (1994) World Ocean Atlas 1994. Volume 4: temperature. NOAA Atlas NESDIS 4. US Department of Commerce, Washington, D.C., USA, pp 117

Liu Y (1996) Modeling the emissions of nitrous oxide and methane from the terrestrial biosphere to the atmosphere. MIT Joint Program on the Science and Policy of Global Change. Rep 10, MIT, USA

Manabe S, Stouffer RJ (1988) Two stable equilibria of a coupled ocean–atmosphere model. J Clim 1: 841–866

Manabe S, Stouffer RJ (1994) Multi-century response of a coupled ocean–atmosphere model to an increase of atmospheric carbon dioxide. J Clim 7: 5–23

McDougall TJ, Hirst AC, England MH, McIntosh PC (1996) Implications of a new eddy parametrization for ocean models. Geophys Res Lett 23: 2085–2088

Mikolajewicz U, Voss R (2000) The role the individual air-sea flux components in $CO_2$-induced changes of the ocean's circulation and climate. Clim Dyn 16: 627–642

Mitchell JFB, Johns TC, Senior CA (1998) Transient response to increasing greenhouse gases using model with and without flux adjustment. Hadley Centre Technical Note 2, UK

Opsteegh JD, Haarsma RJ, Selten FM, Kattenberg A (1998) A dynamic alternative to mixed boundary conditions in ocean models. Tellus 50A: 348–367

Paiva AP, Chassignet EP (2001) The impact of surface flux parameterizations on the modeling of the North Atlantic ocean. J Phys Oceanogr 31: 1860–1879

Pacanowski R, Dixon K, Rosati A (1995) The GFDL Modular Ocean Model 2 users guide version 1.0, GFDL Ocean Group Technical Report 3, NOAA/Geophysical Fluid Dynamics Laboratory, Princeton, NJ, USA

Perry GD, Duffy PB, Miller NL (1996) An extended data set of river discharges for validation of general circulation models. J Geophys Res 101: 21,339–21,349

Petouchov V, Ganapolski A, Brovkin V, Claussen M, Eliseev A, Kubatzki C, Rahmstorf S (2000) CLIMBER-2: aclimate system model of intermediate complexity. Part I: model description and performance for present climate. Clim Dyn 16: 1–17

Prinn R, Jacoby H, Sokolov A, Wang C, Xiao X, Yang Z, Eckaus R, Stone P, Ellerman D, Melillo J, Fitzmaurece J, Kicklighter D, Holian G, Liu Y (1999) Integrated global system model for climate policy assessment: feedbacks and sensitivity studies. Climatic Change 41: 469–546

Reeh N (1994) Calving from Greenland glaciers: observations, balance estimates of calving rate, calving laws. Workshop on the calving rate of West Greenland glaciers in response to climate change. Danish Polar Center, Copenhagen, pp 171

Reilly J, Prinn R, Fitzmaurece J, Jacoby H, Kicklighter D, Melillo J, Stone P, Sokolov A, Wang C (1999) Multi-gas assessment of the Kyoto Protocol. Nature 401: 549–555

Rivin I, Tziperman E (1997) Sensitivity of air-sea fluxes to SST perturbations. J Clim 10: 2431–2446

Russell GL, Miller JR, Tsang L-C (1985) Seasonal ocean heat transport computed from an atmospheric model. Dyn Atmos Oceans 9: 253–271

Schmitt RW, Bogden PS, Dorman CE (1989) Evaporation minus precipitation and density fluxes for the NA. J Phys Oceanogr 19: 1208–1221

Schmittner A, Stocker TF (1999) The stability of the thermohaline circulation in global warming experiments, J Clim 12: 1117–1133

Sokolov AP, Stone PH (1995) Description and validation of the MIT version of the GISS 2D model, MIT Joint Program on the Science and Policy of Global Change. Rep 2, MIT

Sokolov A, Stone P (1998) A flexible climate model for use in integrated assessments. Clim Dyn 14: 291–303

Sokolov AP, Forest CE, Stone PH (2001)) A comparison of the behavior of different AOGCMs in transient climate change experiments. MIT Joint Program on the Science and Policy of Global Change Rep

Stocker TF, Wright DG, Mysak LA (1992) A zonally averaged, coupled ocean–atmosphere model for paleoclimate studies, J Clim 5: 773–797

Stone P, Yao M-S (1987) Development of a two-dimensional zonally averaged statistical–dynamical model. Part II: the role of eddy momentum fluxes in the general circulation and their parametrization. J Atmos Sci 44: 3769–3536

Stone P, Yao M-S (1990) Development of a two-dimensional zonally averaged statistical–dynamical model. Part III: the parametrization of the eddy fluxes of heat and moisture. J Clim 3: 726–740

Stouffer RJ, Manabe S (1999) Response of a coupled ocean–atmosphere model to increasing atmospheric carbon dioxide: sensitivity to the rate of increase. J Clim 12: 2224–2237

Trenberth KE (1998) The heat budget of the atmosphere and ocean. Proc First Int Conf Reanalysis, Silver Spring MD, USA, 27–31 October 1997

Trenberth KE, Solomon A (1994) The global heat balance: the heat transports in the atmosphere and ocean, Clim Dyn 9: 107–134

Trenberth KE, Olson JG, Large WG (1989) A global ocean wind stress climatology based on ECMWF analysis. NCAR Tech Note, NCAR/TN-338 + STR

Voss R, Sausen R, Cubasch U (1998) Periodically synchronouslly coupled integration with the atmosphere–ocean general circulation model ECHAM3/LSG. Clim Dyn 14: 249–266

Wang C, Prinn RG, Sokolov AP (1998) A global interactive chemistry and climate model. J Geophys Res 103(D3): 3399–3417

Weaver AJ, Hughes TMC (1996) On the incompatibility of ocean and atmosphere models and the need for flux adjustments. Clim Dyn 12: 141–170

Webster MD, Forest CE, Reilly JM, Sokolov AP, Stone PH, Jacoby HD, Prinn RG (2001) Uncertainty analysis of global climate change projections, MIT Joint Program on the Science and Policy of Global Change. Rep 3, pp 3

Wiebe EC, Weaver AJ (1999) On the sensitivity of global warming experiments to the parametrization of sub-grid scale ocean mixing. Clim Dyn 15: 875–893

Wood RA, Keen AB, Mitchell JFB, Gregory JM (1999) Changing spatial structure of the thermohaline circulation in response to atmospheric $CO_2$ forcing in a climate model. Nature 399: 572–575

Xiao X, Kicklighter D, Melillo J, McGuire D, Stone P, Sokolov A (1997) Linking a global terrestrial biogeochemical model with a 2-dimensional climate model: implication for the global carbon budget. Tellus 49B: 18–37